Determination of power-law attenuation coefficient and dispersion spectra in multi-wall carbon nanotube composites using Kramers–Kronig relations

Joel Mobley[a)]
Department of Physics and Astronomy and Jamie Whitten National Center for Physical Acoustics, University of Mississippi, 1 Coliseum Drive, University, Mississippi 38677

Richard A. Mack
Jamie Whitten National Center for Physical Acoustics, University of Mississippi, 1 Coliseum Drive, University, Mississippi 38677

Joseph R. Gladden
Department of Physics and Astronomy, University of Mississippi, 108 Lewis Hall, University, Mississippi 38677

P. Raju Mantena
Department of Mechanical Engineering, University of Mississippi, 201D Carrier Hall, University, Mississippi 38677

(Received 14 October 2008; revised 2 January 2009; accepted 2 April 2009)

Using a broadband through-transmission technique, the attenuation coefficient and phase velocity spectra have been measured for a set of multi-wall carbon nanotube (MWCNT)-nylon composites (from pure nylon to 20% MWCNT by weight) in the ultrasonic frequency band from 4 to 14 MHz. The samples were found to be effectively homogeneous on spatial scales from the low end of ultrasonic wavelengths investigated and up (>0.2 mm). Using Kramers–Kronig relations, the attenuation and dispersion data were found to be consistent with a power-law attenuation model with a range of exponents from $y=1.12$ to $y=1.19$ over the measurement bandwidth. The attenuation coefficients of the respective samples are found to decrease with increasing MWCNT content and a similar trend holds also for the dispersion. In contrast, the mean phase velocities for the samples rise with increasing MWCNT content indicating an increase in the mechanical moduli.
 [DOI: 10.1121/1.3125323]

PACS number(s): 43.35.Cg, 43.20.Jr, 43.35.Yb, 43.35.Zc [RLW] Pages: 92–97

I. INTRODUCTION

Since the discovery of carbon nanotubes (CNTs) by Iijima in 1991,[1] significant efforts have been made to incorporate these nanoparticles with conventional materials in order to improve the mechanical strength and stiffness or other physical properties (e.g., electrical and thermal conductance) of the resulting composite.[2–4] CNTs include both single- and multi-walled (MWCNT) structures, with the former having typical outside diameter (OD) of 1–2 nm while the latter an OD of 8–12 nm. Their lengths range from the typical 10 μm to as much as 100 μm with very high aspect ratios (length-to-diameter) of order 1000:1. CNTs have about 50 times the tensile strength of stainless steel (100 GPa vs 2 GPa) and five times the thermal conductivity of copper. Incorporating nano-scale particles into a matrix to construct a macro-scale composite can potentially offer improved performance over composites with larger inclusions (e.g., conventional carbon fibers) for several reasons, including the increased effective surface area of contact between the nanoparticles and the matrix, and higher crystallinity. CNT composites aim to capitalize on both the extraordinary mechanical properties of the individual CNTs and the potential advantages of nanoscale reinforcing particles. Research on CNT composites is diverse incorporating a variety of matrix materials and CNT types and sizes. Realizing the promise of enhanced mechanical properties relies on the ability to disperse the CNTs uniformly in the host material and on achieving good interfacial bonding for transferring loads across the matrix-fiber interface.[2–4] The dynamic properties of composite materials in the ultrasonic region of the spectrum can provide information about the mechanical moduli, fiber/matrix coupling, and structural integrity of composite materials.[5–8] The attenuation spectra of ultrasonic stress waves are sensitive to the coupling of the matrix and reinforcing inclusion as well as the homogeneity over length scales relevant for structural applications. The phase velocity spectra can be used to determine the dynamic mechanical moduli of a material, while the velocity dispersion is linked to the attenuation (as discussed below) and thus sensitive to a similar list of properties. Nonlinear mechanical properties of composites can also be used to find signs of microstructural degradation.[9]

Broadband ultrasonic spectroscopy is a technique utilizing time-localized signals to determine the phase velocity and attenuation coefficient spectra over a range of frequen-

[a)]Author to whom correspondence should be addressed. Electronic mail: jmobley@olemiss.edu

cies simultaneously.[10] The attenuation coefficient and phase velocity spectra are components of the complex wavenumber and are further interlinked through the Kramers–Kronig (KK) relations. Fundamentally rooted in causality, KK relations provide linkages between the physical properties that govern the response of matter and materials to external stimuli. Due to their general foundations[11] KK relations have proven to be adaptable and applicable to a wide array of tasks which include measuring fundamental material parameters, establishing the consistency of laboratory data, and building causally-consistent physical models. KK relations between components of the complex wavenumber using the method of subtractions have been established for both homogeneous and inhomogeneous materials.[12] One complication in adapting KK relations for the analysis of data is the knowledge gap that exists between the infinite bandwidth required by the KK integrals and the measured data which are inherently bandlimited. The impact of this gap on KK calculations depends on many factors, both general and system-dependent. However, finite bandwidth approximations to the KK relations have proven to be applicable to measured ultrasonic attenuation and velocity spectra for suspensions exhibiting resonant features,[13–16] and have also proven accurate for the analysis of systems exhibiting monotonic behavior where the attenuation varies as a frequency power-law over limited experimental bandwidths.[17,18] For the power-law attenuation, the KK relations predict that the velocity dispersion also varies as a power-law (or logarithmically in the case that the attenuation is linear in frequency), although with a scaling factor that is a function of the power-law exponent.[17,19] Due to convergence problems with a KK formulation in use at the time, these results were first derived with an alternate technique, known as the time-causal method.[19] Using the method of subtractions,[12,20] the convergence problems were circumvented permitting valid KK calculations to be performed. In this work, we present data for the attenuation coefficient and phase velocity spectra of longitudinal mode elastic waves in the ultrasonic frequency regime for a series of nylon matrix materials containing various concentrations of MWCNTs. The attenuation coefficient spectra for the samples examined in this work are found to follow a power-law dependence on frequency and the dispersion data exhibits the variation predicted by the KK relations.

II. THEORY

In a variety of media (including some liquids, soft mammalian tissues, and solid polymers) over a finite bandwidth, the attenuation coefficient of ultrasonic waves appears to be adequately modeled by a power-law dependence on frequency

$$\alpha(f) = \alpha_0 |f|^y, \tag{1}$$

where α_0 and y are real constants, with $1 \leq y \leq 2$. The frequency response of a medium of thickness h can be characterized by its transfer function

TABLE I. The densities of the samples examined in this work.

Sample	Density (g/cm^3)
20% MWCNT	1.25
10% MWCNT	1.20
5% MWCNT	1.17
Nylon (0% MWCNT)	1.14

$$H(f,h) = \exp[iK(f)h], \tag{2}$$

where

$$K(f) = \frac{2\pi f}{c_p(f)} + i\alpha(f) \tag{3}$$

is the conventional complex wavenumber, and $c_p(f)$ is the phase velocity. Given that the power-law attenuation persists throughout the spectrum, the KK relations predict that the phase velocities at two frequencies f and f_0 have the following relationship:[17,19]

$$\frac{1}{c_p(f)} = \frac{1}{c_p(f_0)} + \frac{\alpha_0}{2\pi}\tan\left(y\frac{\pi}{2}\right)(|f|^{y-1} - |f_0|^{y-1}) \quad \text{for} \quad 1 < y \leq 2, \tag{4a}$$

which takes the form

$$\frac{1}{c_p(f)} = \frac{1}{c_p(f_0)} - \frac{\alpha_0}{\pi^2}\ln\left|\frac{f}{f_0}\right| \quad \text{in the limit } y \to 1. \tag{4b}$$

These causally-consistent functional forms for the attenuation and phase velocity spectra have been shown to accurately describe the behavior of real materials over band limited windows in the low-megahertz region of the acoustic spectrum.[17–19]

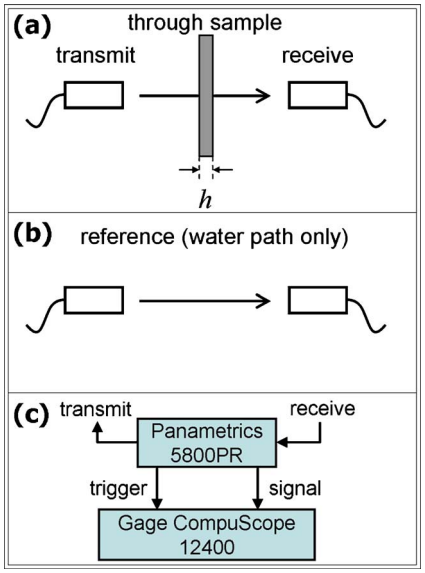

FIG. 1. (Color online) (a) The through sample and (b) reference (water path only) signal acquisition steps of the substitution method. (c) Schematic diagram of the instrumentation in the measurement system.

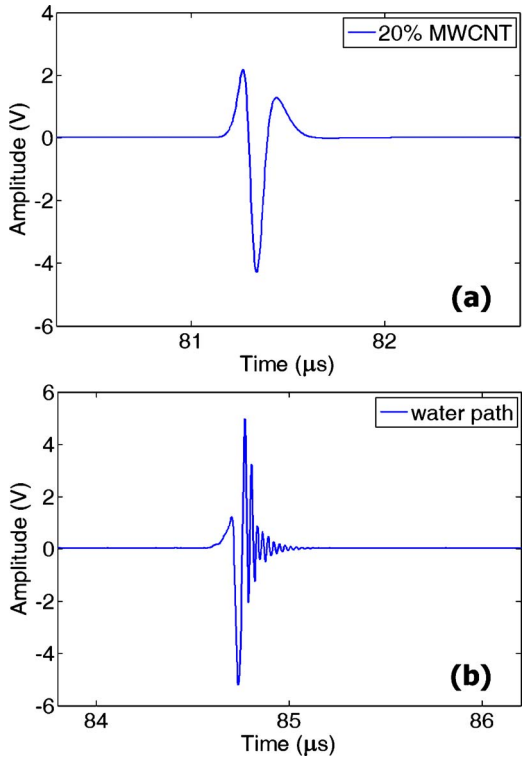

FIG. 2. (Color online) Representative waveforms captured during (a) through-sample acquisition (20% MWCNT sample) and (b) reference (water path only) acquisition.

III. MATERIALS

The samples were provided as extruded plates by Ensinger Inc. with weight fractions of MWCNTs of 0% (pure nylon), 5%, 10%, and 20%. The polymer matrix for the samples is nylon 6,6. The MWCNTs were produced by Hyperion Catalysis International, Inc. (Cambridge, MA). The densities of the samples are shown in Table I.

IV. DATA ACQUISITION AND ANALYSIS

The velocity and attenuation data were determined using the broadband ultrasonic spectroscopy technique implemented in a through-transmission set-up, as shown in Fig. 1. The ultrasound was generated and received by a pair of PVDF transducers (Olympus NDT/Panametrics) immersed in a water bath and separated by 12.5 cm. The transmitter was excited by a broadband pulser/receiver unit (Olympus NDT/Panametrics 5800). The received signals were captured by a digital oscilloscope (GaGe Applied Compuscope 12400) where they were digitized to 12 bits at a rate of 400 Msamples/s. For each sample, through-transmitted ultrasonic signals were acquired [Fig. 1(a)] from five sites at normal incidence. A representative through-sample waveform is shown in Fig. 2(a). In addition to the through-sample acquisitions, waterpath only waveforms were captured to serve as the reference data in the analysis, as shown in Fig. 1(b). A captured signal from a waterpath only acquisition is shown in Fig. 2(b). Sample thicknesses were measured ultrasonically at each acquisition site on the sample and are derived from time-of-flight measurements from pulse-echo signals off the near sample face for each transducer and a waterpath

TABLE II. The fit values for the attenuation constant, the exponent of the power law attenuation coefficients, and the offset a_0 for the four samples.

Sample	α_0 (Np mm^{-1} MHz^{-y})	y	a_0 (Np/mm)
20% MWCNT	0.0217	1.169	0.0108
10% MWCNT	0.0272	1.123	−0.0048
5% MWCNT	0.0264	1.154	–0.0046
Nylon (0% MWCNT)	0.0267	1.187	−0.0038

only through-transmission acquisition.[21] Waveform data were acquired by accumulating 5000 raw signals and the accumulated signal was recorded to disk for further processing. The discrete Fourier transforms of the through-transmitted and waterpath signals were taken, and the amplitude and phase spectra from each were then used to compute the attenuation coefficient and phase velocity for each site on a given sample. The attenuation coefficient was determined using the following relation:

$$\alpha(f) = \alpha_w(f) + \frac{\ln \frac{A_{\text{ref}}(f)}{A_{\text{thru}}(f)} + \ln T}{h}, \tag{5}$$

where $\alpha_w(f)$ is the attenuation coefficient for water, $A_{\text{thru}}(f)$ and $A_{\text{ref}}(f)$ are the Fourier amplitude spectra of the through-sample and reference waveforms, respectively, h is the sample thickness, and $T=4Z_wZ_s/(Z_w+Z_s)^2$ is the single-pass

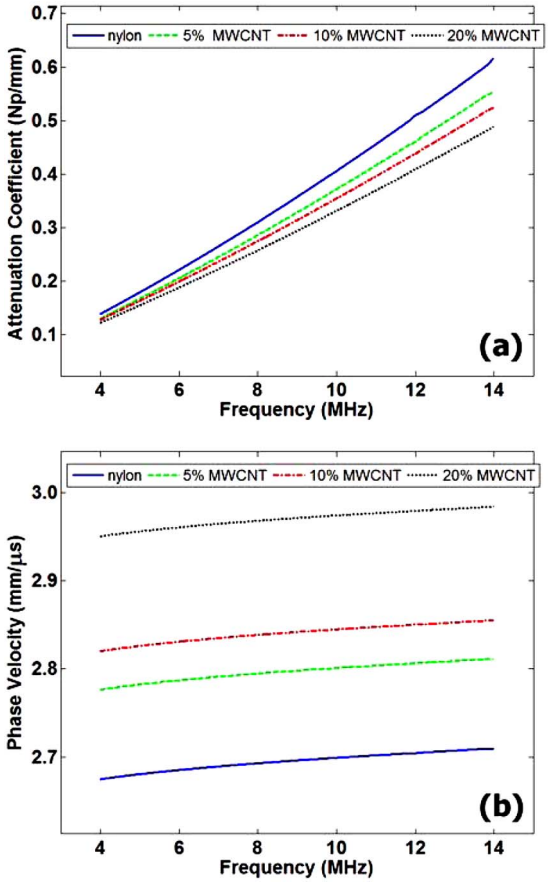

FIG. 3. (Color online) The measured (a) attenuation coefficient and (b) phase velocity spectra for the four samples studied in this work.

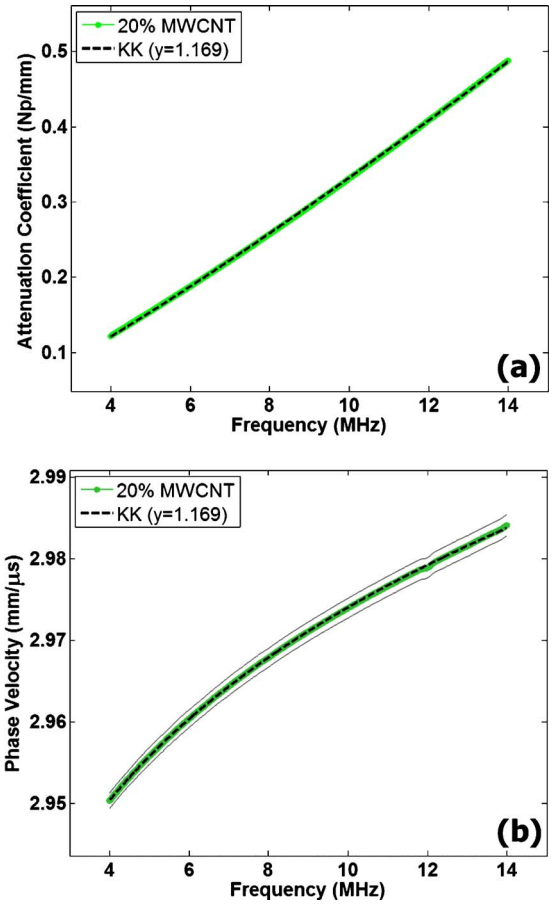

FIG. 4. (Color online) The experimental attenuation coefficient and phase velocity spectra for the 20% MWCNT sample with their associated KK predicted curves. The solid lines in the bottom panel are the standard deviation limits of the measured quantities. (The standard deviation limits for the attenuation data are smaller than the width of the plotted curve.)

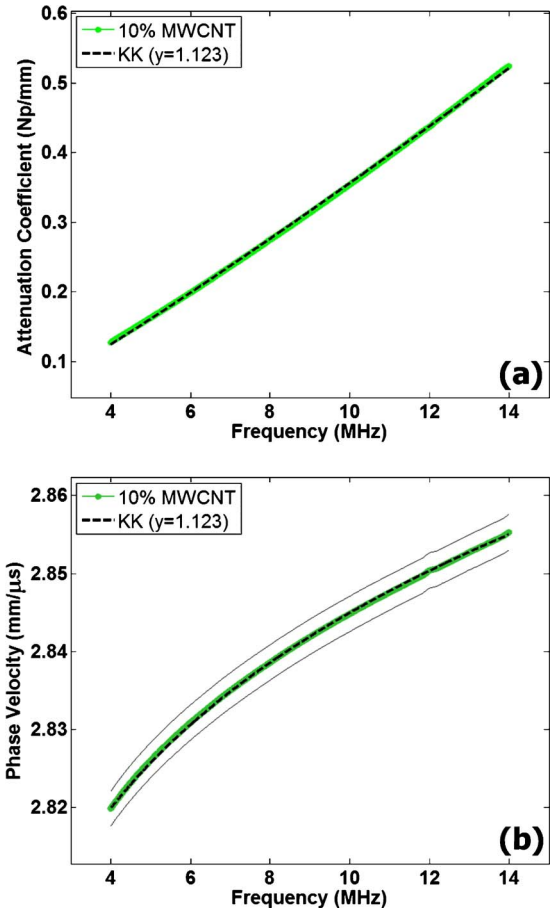

FIG. 5. (Color online) The experimental attenuation coefficient and phase velocity spectra for the 10% MWCNT sample with their associated KK predicted curves. The solid lines in the bottom panel are the standard deviation limits of the measured quantities. (The standard deviation limits for the attenuation data are smaller than the width of the plotted curve.)

amplitude transmission coefficient including both the entry and exit water/sample interfaces, where $Z_w = \rho_w c_w$ and $Z_w = \rho_s c_p(f)$ are the characteristic acoustic impedances of the water and the sample, respectively (the sample densities, $\{\rho_s\}$, are given in Table I). The phase velocity relation is

$$c(f) = \frac{c_w}{1 - c_w \dfrac{\Delta\phi(f)}{2\pi f h}}, \tag{6}$$

where $\Delta\phi(f) = \phi_{\text{thru}}(f) - \phi_{\text{ref}}(f)$ is the difference in the unwrapped phase spectra from the two signals compensated for sheet offsets. The speed of sound in water, c_w, was determined by the water temperature using the formula from Ref. 22.

After the attenuation coefficient and phase velocity spectra were measured at five sites on a given sample, the spectra were averaged across the sites to yield a single attenuation and velocity spectrum for each sample. To determine the parameters α_0 and y in each case, the attenuation data were fitted to a model function of the form $\alpha(f) = a_0 + \alpha_0 f^y$, where a_0 is the offset of the attenuation data at zero frequency (beyond the low frequency limits of the measurement spectrum). This was done over a range of exponents from $y = 1.001$ to $y = 1.349$, and the exponent y and associated coefficient α_0 that gave the best fit to the dispersion data using Eq. (4a) were used. The values for the parameters α_0 and y as determined by this procedure are given in Table II. (See Table III for phase velocity values at $f_{\text{low}} = 4$ MHz.)

V. RESULTS AND DISCUSSION

The results for the attenuation coefficient and phase velocity for all four samples are shown together in the panels of Fig. 3. The comparisons of the measured attenuation and dispersion data with the KK power-law model predictions are shown for each respective sample in Figs. 4–7. The top panel in each of Figs. 4–7 shows the attenuation coefficient and its power-law fit. The bottom panel in each figure compares the measured phase velocity spectra with the KK prediction in the form of Eq. (4a) using the parameters from the attenuation fit.

The attenuation coefficient spectrum for the pure nylon sample exhibited the highest values throughout the measurement bandwidth, and across the samples the attenuation was found to decrease with increasing MWCNT content (in the same way as with the dispersion as discussed below), as shown in Fig. 3(a). The attenuation coefficient of the nylon-only sample also exhibited the steepest rise with frequency, and the largest power-law exponent of about 1.19. The at-

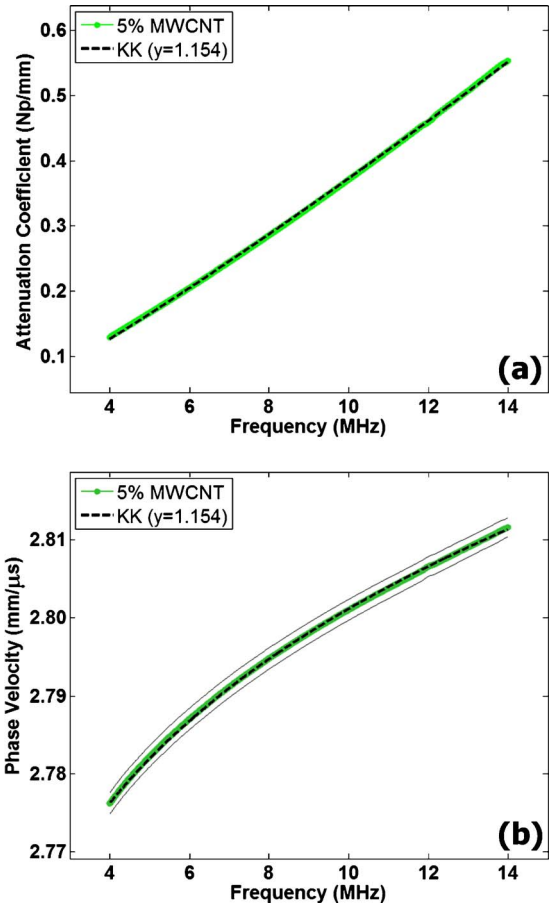

FIG. 6. (Color online) The experimental attenuation coefficient and phase velocity spectra for the 5% MWCNT sample with their associated KK predicted curves. The solid lines in the bottom panel are the standard deviation limits of the measured quantities. (The standard deviation limits for the attenuation data are smaller than the width of the plotted curve.)

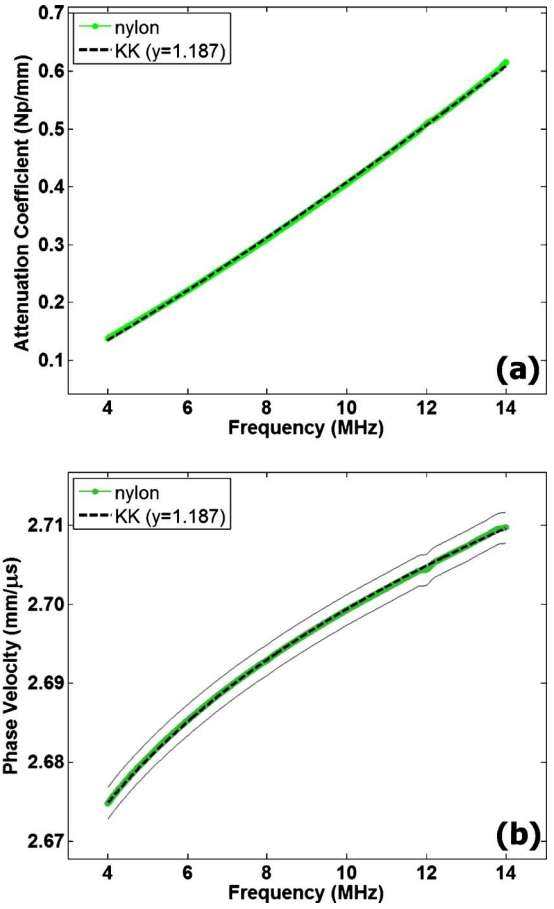

FIG. 7. (Color online) The experimental attenuation coefficient and phase velocity spectra for the nylon (0% MWCNT) sample with their associated KK predicted curves. The solid lines in the bottom panel are the standard deviation limits of the measured quantities. (The standard deviation limits for the attenuation data are smaller than the width of the plotted curve.)

tenuation coefficient of the 20% MWCNT sample was the smallest among the samples across the spectrum and the slowest rise with frequency. The power-law exponent of the 5% MWCNT sample and 10% MWCNT sample fell monotonically from the nylon value, but the 20% MWCNT sample had a greater exponent than both the 5% and 10% MWCNTs while still remaining lower than the nylon-only. The reasons for the monotonic decrease in attenuation with increasing MWCNT concentration are not clear, although this could due to differences in the bulk attenuation of the two media (volume related effect) or some aspect of the coupling between the two phases (interphase boundary effects and scaling with the interphase surface area). Simple series- and parallel-type volumetric law of mixtures models were unable to account for the differences in attenuation among the samples. It is likely that a combination of factors contributes to the observed trend, but a more definitive judgment on this manner is beyond the scope of the present work.

The phase velocity and dispersion results are summarized in Table III. The mean phase velocities (averaged across the 4–14 MHz bandwidth) for the four samples exhibit an increase as MWCNT content rises, starting from a value of 2.695 mm/μs for the pure nylon (0% MWCNT) sample up to 2.970 mm/μs for the 20% MWCNT sample. This is indicative of an increase in the Young's modulus of about 28% from pure nylon to the composite with the highest fraction of MWCNT, assuming that nylon's Poisson's ratio of about 0.39 continues to hold.[23] The dispersion, defined as $\Delta(1/c)=[1/c(f_{\text{low}})]-[1/c(f_{\text{high}})]$ [as is natural based on the form predicted in Eq. (4)], varies from sample to sample with the dispersion decreasing with increasing MWCNT content. This is the same trend as seen with the attenuation data as expected from the causally-consistent forms of Eqs. (3) and (4). (An interesting observation is that the change in phase velocity, $\Delta c=c(f_{\text{high}})-c(f_{\text{low}})$, as dispersion is often defined, did not change significantly from sample to sample.) The pure nylon exhibited the greatest dispersion, with a variation in $\Delta(1/c)$ about 1.26 times higher than that of the 20% MWCNT sample. These dispersion data are also consistent with the attenuation coefficient determinations as linked by the KK relations, as can be seen in the Figs. 4(b), 5(b), 6(b), and 7(b). In each case the KK prediction is almost indistinguishable from the measured phase velocity. It is clear that the KK predicted forms are quantitatively consistent with these data. It is not clear, however, how far beyond the measurement bandwidth one could expect these forms to continue to hold.

VI. CONCLUSION

The phase velocity and attenuation coefficient spectra of composite materials with varying amounts of MWCNT con-

TABLE III. Phase velocity measurements from the four samples. The first three columns are the values at 4, 9, and 14 MHz, respectively. The fourth column is the phase velocity averaged over the entire bandwidth, and the last column is the dispersion.

Sample	$c_p(f_{\text{low}})$ (mm/μs)	$c_p(f_{\text{median}})$ (mm/μs)	$c_p(f_{\text{high}})$ (mm/μs)	$\bar{c}_p$ (mm/μs)	$1/c_p(f_{\text{low}})-1/c_p(f_{\text{high}})$ (mm/μs)$^{-1}$
20% MWCNT	2.950	2.971	2.984	2.970	3.83×10^{-3}
10% MWCNT	2.820	2.842	2.855	2.840	4.40×10^{-3}
5% MWCNT	2.776	2.798	2.812	2.797	4.53×10^{-3}
Nylon (0% MWCNT)	2.675	2.696	2.710	2.695	4.82×10^{-3}

tent (from 0 to 20% by weight) were measured using a broadband technique. The samples were found to be effectively homogeneous on spatial scales from the low end of ultrasonic wavelengths investigated and up (>0.2 mm). Over the measurement bandwidth, these spectra were found to be a consistent KK model that utilizes a frequency power-law form for the attenuation coefficient. The mean phase velocity increased monotonically with the rising MWCNT content, indicating an increase in the mechanical moduli with MWCNT concentration. The attenuation coefficient and the dispersion both showed the opposite trend, decreasing with increasing MWCNT content, consistent with the predictions of the KK model.

ACKNOWLEDGMENT

Support for this research by the Office of Naval Research, Solid Mechanics Program, ONR Grant No N00014-07-1-1010 (Dr. Yapa D. S. Rajapakse, Program Manager), is acknowledged.

[1]S. Iijima, "Helical microtubules of graphitic carbon," Nature (London) **354**, 56–58 (1991).
[2]P. J. F. Harris, "Carbon nanotube composites," Int. Mater. Rev. **49**, 31–43 (2004).
[3]J. N. Coleman, U. Khan, W. J. Blau, and Y. K. I. Gun'ko, "Small but strong: A review of the mechanical properties of carbon nanotube-polymer composites," Carbon **44**, 1624–1652 (2006).
[4]J. Njuguna, K. Pielichowski, and J. R. Alcock, "Epoxy-based fibre reinforced nanocomposites," Adv. Eng. Mater. **9**, 835–847 (2007).
[5]S. I. Rokhlin, W. Huang, and Y. C. Chu, "Ultrasonic scattering and velocity methods for characterization of fiber-matrix interphases," Ultrasonics **33**, 351–364 (1995).
[6]Y. C. Chu and S. I. Rokhlin, "Determination of macromechanical and micromechanical and interfacial elastic properties of composites from ultrasonic data," J. Acoust. Soc. Am. **92**, 920–931 (1992).
[7]K. Balasubramaniam, S. Alluri, P. Nidumolu, P. R. Mantena, J. G. Vaughan, and M. Kowsika, "Ultrasonic and vibration methods for the characterization of pultruded composites," Composites Eng. **5**, 1433–1451 (1995).
[8]J. Wu, C. Layman, S. Murthy, and R.-B. Yang, "Determine mechanical properties of particulate composite using ultrasound spectroscopy," Ultrasonics **44**, e793–e800 (2006).
[9]K. Y. Jhang, "Applications of nonlinear ultrasonics to the NDE of material degradation," IEEE Trans. Ultrason. Ferroelectr. Freq. Control **47**, 540–548 (2000).
[10]W. Sachse and Y.-H. Pao, "On the determination of phase and group velocities of dispersive waves in solids," J. Appl. Phys. **49**, 4320–4327 (1978).
[11]J. S. Toll, "Causality and the dispersion relations: Logical foundations," Phys. Rev. **104**, 1760–1770 (1956).
[12]R. L. Weaver and Y.-H. Pao, "Dispersion relations for linear wave propagation in homogeneous and inhomogeneous media," J. Math. Phys. **22**, 1909–1918 (1981).
[13]J. Mobley, "Finite-bandwidth Kramers-Kronig relations for acoustic group velocity and attenuation derivative applied to encapsulated microbubble suspensions," J. Acoust. Soc. Am. **121**, 1916–1923 (2007).
[14]J. Mobley, K. R. Waters, and J. G. Miller, "Causal determination of acoustic group velocity and frequency derivative of attenuation with finite-bandwidth Kramers-Kronig relations," Phys. Rev. E **72**, 016604 (2005).
[15]J. Mobley, K. R. Waters, M. S. Hughes, C. S. Hall, J. N. Marsh, G. H. Brandenburger, and J. G. Miller, "Kramers-Kronig relations applied to finite bandwidth data from suspensions of encapsulated microbubbles," J. Acoust. Soc. Am. **108**, 2091–2106 (2000); "Erratum: 'Kramers-Kronig relations applied to finite bandwidth data from suspensions of encapsulated microbubbles [J. Acoust. Soc. Am. 108, 2091–2106 (2000)]'," J. Acoust. Soc. Am. **112**, 760–761 (2002).
[16]J. Mobley and R. E. Heithaus, "Ultrasonic properties of a suspension of microspheres supporting negative group velocities," Phys. Rev. Lett. **99**, 124301 (2007).
[17]K. R. Waters, M. S. Hughes, J. Mobley, G. H. Brandenburger, and J. G. Miller, "On the applicability of Kramers–Kronig relations for media with ultrasonic attenuation obeying a frequency power law," J. Acoust. Soc. Am. **108**, 556–563 (2000).
[18]K. R. Waters, M. S. Hughes, J. Mobley, and J. G. Miller, "Differential forms of the Kramers–Kronig dispersion relations," IEEE Trans. Ultrason. Ferroelectr. Freq. Control **50**, 68–76 (2003).
[19]T. L. Szabo, "Causal theories and data for acoustic attenuation obeying a frequency power law," J. Acoust. Soc. Am. **97**, 14–24 (1995).
[20]H. M. Nussenzveig, *Causality and Dispersion Relations* (Academic, New York, 1972).
[21]D. K. Hsu and M. S. Hughes, "Simultaneous ultrasonic velocity and sample thickness measurement and application in composites," J. Acoust. Soc. Am. **92**, 669–675 (1992).
[22]W. Marczak, "Water as a standard in the measurements of speed of sound in liquids," J. Acoust. Soc. Am. **102**, 2776–2779 (1997).
[23]G. S. Kino, *Acoustic Waves: Devices, Imaging, and Analog Signal Processing* (Prentice-Hall, Inc., Englewood Cliffs, NJ, 1987), p. 550.